Hindawi
Advances in Materials Science and Engineering
Volume 2019, Article ID 3165096, 13 pages
https://doi.org/10.1155/2019/3165096

Research Article

Deformation and Failure Characteristics of Soil-Rock Mixture considering Material Composition and Random Structure

Shengnian Wang[1], **Tingting Ji**[1], **Qinpei Xue**[1], **Zhifu Shen**[1] and **Qiang Zhang**[2]

[1]*Institute of Geotechnical Research, Nanjing Tech University, Nanjing 211816, China*
[2]*China Institute of Water Resources and Hydropower Research, Beijing 100038, China*

Correspondence should be addressed to Zhifu Shen; zhifu.shen@njtech.edu.cn

Received 20 March 2019; Revised 9 May 2019; Accepted 22 May 2019; Published 7 October 2019

Academic Editor: Luigi Nicolais

The soil-rock mixture is a cohesive-frictional geomaterial subjected to impacts of composition and structure seriously. When it suffers from gravity or other kinds of loadings, the loss of its bearing capacity always appears a progressive failure. In this study, the ultimate criterion of the frictional material changing from the deformation stage to the failure stage is analyzed first and then the deformation and failure characteristics of the soil-rock mixture with different compositions and structures are discussed by the discrete element method. The results indicate that the deformation and failure of the soil-rock mixture under axial pressure appear a significant phenomenon of detouring around rock blocks. The bond failure zones and the ultimate shear strain increase with the increase of rock block proportion. The distribution of the bond failure zones always has a good uniformity with the inclination of rock block inclinations. The increase of cementation degree between particles expands the distribution of the bond failure zones but minifies the ultimate shear strain.

1. Introduction

Soil-rock mixture (SRM) is a kind of extremely heterogeneous geological material, composed of rock blocks with high stiffness and fine-grained soil with cementation. However, due to inhomogeneous cementation between particles, complex granulometric composition, and random distribution of rock blocks, SRM belongs to neither the category of soil nor rock [1–3]. Holtz and Gibbs [4] as early as 1956 had pointed out that only when the granulometric composition of the reconstituted SRM conforms to the actual conditions could the indoor tests truly reflect their properties. Chandler [5] further indicated that limited experiments in the local area were not very representative because large rock blocks within SRM could significantly increase the shear strength and density. Zhai et al. [6] showed that the strength of residual soils can be related to the physical and mechanical properties of their rock fragments. Therefore, researches on the properties of SRM should take material composition and structural features into consideration.

Experimental investigation and numerical simulation on physical and mechanical properties of SRM have been widely carried out in recent years, including statistical analysis of granulometric composition [7, 8], direct shear test [9–12], triaxial compression test [13, 14], and water permeability test [15–17]. All of these documents indicate that the existence of rock blocks always leads to special features in the stress-strain curve, shear strength, shear dilatancy, and softening-hardening rules, and the proportion of rock blocks determines the physical and mechanical properties of SRM to a certain extent [18–22]. However, research work on deformation and failure of SRM is quite limited. As a kind of typical frictional geomaterial, the failure of SRM will always undergo a process from elastic deformation to plastic deformation and finally lose its bearing capacity under compression or shear loadings completely. Although the yielding criterion of the

frictional geomaterial, such as the Mohr–Coulomb criterion, gives the condition of material deformation from the linear elastic stage to plastic stage, and it cannot determine whether the material completely loses its bearing capacity under loadings or not. The geomaterial actually still holds a relative high level of capacity to bear loading after plastic yielding and develops the residual deformation. Only when the plastic deformation of the geomaterial develops to its ultimate deformation can the geomaterial truly reach its ultimate bearing capacity [23, 24]. In other words, when SRM reaches its peak strength under gravity or other loadings, the fine particles will first yield plastic deformation locally and cause a reduction of bearing capacity. However, this localized plastic deformation does not mean that the SRM has already lost its ultimate bearing capacity. When the localized plastic deformation continues to increase, the localized plastic zones begin to expand and connect together. Only when the localized plastic zones expand throughout boundaries does SRM truly fail. Therefore, how to define deformation and failure of SRM and give the criteria of SRM from the deformation stage to the failure stage could be much favorable to engineering safety assessment and work out comprehensive treatment more economically and reasonably.

Generally, there are three ways to describe the yield and failure of materials: energy, stress, and strain [25]. The method of energy based on the law of thermodynamics points out that energy transformation is the essential characteristic of the physical process of material. When the material is undergoing continuous deformation, the properties of the material changes with the exchange of energy between inside and outside of the material. The yield and failure of materials can be thus studied in terms of energy. Unfortunately, research work related to the energy yield criterion for geotechnical materials is still less [26]. The method of stress and strain is relatively intuitive, and its specific value can be measured in the test. So they are the most commonly used method in the study of the strength (failure) theory for geomaterials. For examples, Tresca yield criterion and Mohr–Coulomb yield criterion belong to the shear yield criterion for the shear stress and the normal stress at the critical plane of a given material point; Mises yield criterion and Drucker–Prager yield criterion belong to the shear yield criterion for the comprehensive measurement of shear stress and normal stress of all planes of a given material point [27]; the Lade–Duncan single-yield surface model mainly reflects the shear yield but does not fully reflect the volume yield [28]. However, the SRM is a kind of multiphase friction material composed of particles. The deformation of them is originated from the relative displacement among particles, which results in the original transmission capacity between the particle reducing. Hence, it is more appropriate to use strain to characterize the material's ability to resist relative displacement between mineral particles inside the SRM. The method of strain for describing the yield and failure of concrete had been proposed first by Drucker and Il'yushin in the 1950s, and begun to bear fruit. For examples, previous researches suggest that the ultimate strain used to judge the yield and failure of metal materials had been proved to be very effective [29, 30]; Mou et al. [31] had studied the influence of the distribution and magnitude of the plastic strain on the mode and position of deformation and failure; Polak [32] indicated that the microcrack propagation is related to plastic strain; Jie et al. [33] validated the feasibility and validity of the ultimate strain to describe the failure and cracking of material points under dynamic loads. However, these studies mainly focused on brittle ailure. Outcomes about the ductile shear failure of the soil and rock material are very limited and are no exceptions to SRM. Therefore, it is very necessary to do a study in strain criterion of ductile shear failure for SRM.

In this study, the ultimate criterion of SRM changing from the deformation stage to the failure stage is analyzed based on the ideal elastic-plastic model first and then the deformation and failure of reconstructed SRM taking material composition and structural features into consideration are simulated by a series of numerical uniaxial compression tests. Finally, the impacts of material compositions and structural features on the ultimate criteria of SRM are discussed.

2. Ultimate Criterion of Material Failure

The strains of the geomaterial that applied an ideal elastic-plastic model in theory will increase infinitely with constant stress when this material fails. However, since the yielding and failure criteria are considered as the same, it is difficult to distinguish the yielding and the failure of the geomaterial. If the stress-strain curve of the geomaterial adopts the expression form of strain, the ultimate elastic strain actually is the one that the geomaterial begins to generate plastic deformation in local. Although the geomaterial after elastic deformation has already changed in terms of the properties, it could still hold bearing capacity at a relatively high level. The reason is that the yielding at a point does not represent the failure of the whole material. When the geomaterial using an ideal elastic-plastic model begins to yield plastic deformation, the failures of local zones will be constrained by the surrounding unyielding material. Only if the localized failure zones expand throughout boundaries or the shear strain of the geomaterial reaches its ultimate value does the geomaterial truly fail. Therefore, a better way for estimating the failure of the geomaterial is needed [34].

Normally, there must be a relationship between the compressive strain and shear strain of geotechnical materials. If the geomaterial meets the ideal elastic-plastic model, the influence of the intermediate principal stress on the behavior of the geomaterial is ignored, and the relationship between the compressive strain and shear strain of the Mohr-Coulomb failure criterion can be expressed as

$$\frac{\varepsilon_1 - \varepsilon_3}{2} - \frac{\varepsilon_1 + \varepsilon_3}{2} \sin\varphi = \gamma_s \cos\varphi + \frac{3\nu}{1 - 2\nu} \varepsilon_m \sin\varphi, \quad (1)$$

where $\varepsilon_m = (\varepsilon_1 + \varepsilon_2 + \varepsilon_3)/3$, ε_1 and ε_3 are the first and third principal strain, $\gamma_s = c(1 + \nu)/E$, c is the cohesion, φ is the

internal friction angle, E is the elasticity modulus, and ν is Poisson's ratio.

When the geotechnical material is under triaxial stress conditions, the elastic ultimate principal strain should meet

$$\varepsilon_{1y} = \frac{\sigma_1 - 2\nu\sigma_3}{E},$$
$$\varepsilon_{2y} = \varepsilon_{3y} = \frac{(1-\nu)\sigma_3 - \nu\sigma_1}{E}. \tag{2}$$

Substituting equation (2) into equation (1), the elastic ultimate principal strain can be expressed as

$$\varepsilon_{1y} = \frac{2c\cos\varphi + [1+\sin\varphi - 2\nu(1-\sin\varphi)]\sigma_3}{E(1-\sin\varphi)},$$
$$\varepsilon_{3y} = \frac{-2\nu c\cos\varphi + [1-\sin\varphi - 2\nu]\sigma_3}{E(1-\sin\varphi)}. \tag{3}$$

If we use $\sqrt{J_2'}$ to define the shear strain, and suppose $\sigma_2 = \sigma_3$, the elastic ultimate shear strain $\sqrt{J_{2y}'}$ can be expressed as

$$\sqrt{J_{2y}'} = \sqrt{\frac{\left[(\varepsilon_1-\varepsilon_2)^2 + (\varepsilon_2-\varepsilon_3)^2 + (\varepsilon_1-\varepsilon_3)^2\right]}{6}} = \frac{(\varepsilon_{1y} - \varepsilon_{3y})}{\sqrt{3}}. \tag{4}$$

Substituting equation (3) into equation (4), the elastic ultimate shear strain can eventually be rewritten as

$$\sqrt{J_{2y}'} = \frac{2(1+\nu)(c\cos\varphi + \sigma_3\sin\varphi)}{\sqrt{3}E(1-\sin\varphi)}. \tag{5}$$

Here, equation (5) is only appropriate for describing the behavior of the geomaterial before plastic yielding. When the geomaterial enters the plastic state, the shear strain will increase continuously with constant stress and may not converge any longer. Therefore, it is very necessary to find new ways to describe the shear strain after plastic yielding [25, 34].

Theoretically, if we use the three principal strains to describe the state of a point in strain space, the deviatoric shear strain can be expressed as

$$\gamma_\pi = 2\sqrt{e_{ij}e_{ij}} = 2\sqrt{2}\sqrt{J_2'}. \tag{6}$$

If we use the polar coordinates $(r_\varepsilon, \theta_\varepsilon)$ to express the strain state on the deviatoric plane, then

$$r_\varepsilon = \frac{1}{\sqrt{3}}\left[(\varepsilon_1-\varepsilon_2)^2 + (\varepsilon_2-\varepsilon_3)^2 + (\varepsilon_3-\varepsilon_1)^2\right]^{1/2} = \frac{\gamma_\pi}{2},$$
$$\tan\theta_\varepsilon = \frac{2\varepsilon_2 - \varepsilon_1 - \varepsilon_3}{\sqrt{3}(\varepsilon_1 - \varepsilon_3)}. \tag{7}$$

If we use the polar coordinates $(r_\varepsilon, \theta_\varepsilon)$ to express the principal strain, then

$$\varepsilon_1 = \sqrt{\frac{2}{3}}r_\varepsilon \sin\left(\theta_\varepsilon + \frac{2\pi}{3}\right) + \varepsilon_m,$$
$$\varepsilon_2 = \sqrt{\frac{2}{3}}r_\varepsilon \sin\theta_\varepsilon + \varepsilon_m, \tag{8}$$
$$\varepsilon_1 = \sqrt{\frac{2}{3}}r_\varepsilon \sin\left(\theta_\varepsilon - \frac{2\pi}{3}\right) + \varepsilon_m.$$

Similarly, if we use $\sqrt{J_2'}$ to define the shear strain, the principal strain ε_i, the shear strain $\sqrt{J_2'}$, and Lode's angle θ_ε on the deviatoric strain plane will meet:

$$\varepsilon_2 - \varepsilon_m = 2\sqrt{\frac{J_2'}{3}}\sin\theta_\varepsilon. \tag{9}$$

If the geomaterial is isotropic and obeys compression failure on large scales, then $\varepsilon_2 = \varepsilon_3$ and $\theta_\varepsilon = -30^\circ$. Substituting these two conditions into equation (9) yields

$$\sqrt{J_{2f}'} = \frac{(\varepsilon_1 - \varepsilon_2)}{\sqrt{3}}. \tag{10}$$

Since equation (10) expresses a generalized relationship between principal strain and shear strain and meets the expression of the shear strain in the ultimate failure state of geomaterial, it can be applicable for describing the ultimate shear strain of the geomaterial in both triaxial and uniaxial stress states [24, 35]. Considering that the SRM in practical engineering is always distributed near the earth surface or be used as a filling material, in which the confining pressure of them is relatively low, and the strength envelope of SRM after normal consolidation is more approximately a straight line under low confining pressure, a low confining pressure will be applied on the surface of samples before the compression test. Such steps, on the one hand, can simulate the process of soil consolidation and, on the other hand, it ensures that the samples of SRM can be stable under their own weight. The compression test will be carried out by a lower multistage stress loading in final.

3. Random Structure Modeling of SRM

The physical and mechanical properties of SRM are controlled by its material composition and microscopic structure, including granulometric composition, rock block proportion, and inclination. Thus, these three factors will be considered in the modeling of SRM with random structures.

3.1. Definition of Rock Blocks and Its Proportion. SRM can be regarded as a binary mixture of rock blocks and cementitious soil matrix. If we use a grain size threshold to distinguish rock blocks from the cementitious soil matrix, the material composition can be expressed as follows:

$$f = \begin{cases} \text{“rock fragments,”} & d \geq d_{\text{thr}}, \\ \text{“soil matrix,”} & d < d_{\text{thr}}, \end{cases} \tag{11}$$

where d is the equivalent size of the rock block or soil particle and d_{thr} is the threshold grain size.

In fact, many documented research studies have already indicated that SRM exhibits a scale dependency in terms of physical and mechanical properties [36–38]. An approximate linear relationship between grain size and engineering characteristic length has been proposed as

$$d_{\text{thr}} = 0.05L_{\text{c}}, \tag{12}$$

where L_{c} denotes the engineering characteristic length, the value of which is the square root of the sample area for plane problems or the average diameter of the engineering sample for three-dimensional problems. In this study, the simulated sample has a width and height of 40 cm and 80 cm. Therefore, the value of d_{thr} should be approximately 2.83 cm. Here, we take $d_{\text{thr}} = 2$ cm as a conservative size level.

In this study, rock block proportion, R, is defined as the ratio of the rock block area over the sample area for two-dimensional plane problems as follows:

$$R = \sum_{i=1}^{n} \frac{A_i}{A_0}, \tag{13}$$

where A_i is the area of the i^{th} rock block and A_0 is the total area of a SRM sample.

3.2. Geometric Description of Rock Blocks

3.2.1. Size Distribution of Rock Blocks. The typical granulometric curve of SRM with a particle diameter larger than 2 cm is fitted, as shown in Figure 1, in which three representative undisturbed SRM samples had been used for the gradation test. Figure 1 indicates that the chaotic state of SRM's mesostructure is just an external manifestation. The size distribution of rock blocks in SRM actually exhibited a good statistical self-similarity; that is to say, the dimension of the rock blocks in SRM approximately obeys a logarithmic normal distribution [39]. Therefore, the logarithmic normal distribution of particle size will be applied to generate the random rock blocks for the mesostructural reconstruction of SRM.

3.2.2. Shape Description of Rock Blocks. Although rock blocks in nature are in a variety of shapes and sizes, it is still possible to describe their complicated and diversified geometric shapes by random polygons based on some simplifications. Fox example, circle, ellipse, regular, and arbitrary convex polygons nowadays are popular geometries for shape description of rock blocks [40–42]. The core idea of these simulation methods is selecting some specific "basic geometries" first and then zooming or extending these geometries randomly until the final shapes of these generated geometries meet customers' requirements. However, due to the limitations of efficiency in geometric generation and the difficulties in shape description, the randomly generated rock blocks are still different from real rock blocks. In order to improve the generation efficiency of random polygons, an ellipse whose long-axis dimension and ratio of long to short axes obey normal distributions will be used as the initial "basic geometries" in this study. The boundary of this ellipse will be first divided into N segments randomly and then form a convex polygon through connecting adjacent points of these segments for representing rock blocks, as shown in Figure 2. The vertex coordinates of random convex polygon can be expressed as follows:

$$\begin{cases} x_i = x_0 + a\cos\theta_i, \\ y_i = y_0 + a\mu\sin\theta_i, \end{cases} \tag{14}$$

where (x_i, y_i) is the coordinate of the i^{th} vertex of random convex polygon, (x_0, y_0) is the central coordinate of the ellipse, a is the length of ellipse's long axis, μ is the ratio of ellipse's long to short axes, and θ_i is the angle between the long axis of the ellipse and the line connecting the coordinate of the i^{th} vertex of random convex polygon with the central coordinate of the ellipse.

Considering that rock block inclination may also have an impact on the deformation and failure of SRM, the angle between the long axis of the ellipse and the direction of x-axis, α, will be controlled. If the rock block inclination of SRM is unknown, the angle of α can be assumed to obey a random normal distribution, as shown in equation (9). If the rock block inclination of SRM is known, the angle of α will be specified for the known value by users:

$$\begin{cases} x_i' = x_i\cos\alpha - y_i\sin\alpha, \\ y_i' = y_i\cos\alpha + x_i\sin\alpha, \end{cases} \tag{15}$$

where (x_i', y_i') is the coordinate of the i^{th} vertex of random convex polygon after specifying rock block inclination. If the rock block inclination of SRM is indeterminate, $\alpha = \lambda\Delta\varphi, \lambda \in [0, 1), 0 \le \Delta\varphi \le 360^{\circ}$.

3.3. Modeling of SRM with Random Structures

3.3.1. Random Placing Criteria of Rock Blocks. Considering that the distribution of rock blocks within SRM exhibits obvious randomness, random SRM samples considering statistical characteristics shall be more representative. In this study, the central position of rock blocks replaced by random polygons is supposed to obey a random uniform distribution. If r_x and r_y are random numbers independent in statistics, the central position of rock blocks $\{(x, y) \mid x \in [x_{\min}, x_{\max}] \cup y \in [y_{\min}, y_{\max}]\}$ can be expressed as

$$\begin{cases} x_0 = x_{\min} + r_x\left(x_{\max} - x_{\min}\right), \\ y_0 = y_{\min} + r_y\left(y_{\max} - y_{\min}\right). \end{cases} \tag{16}$$

Similarly, considering that rock blocks in SRM are independent mutually, the random placing of rock blocks in a specific region should meet conditions of no overlap, no invasion, and no intersection. If a specific spacing distance between rock blocks is required, the spacing distance should also be adjusted through the distance of two rock blocks.

3.3.2. Invasion Judgment of Rock Blocks. The random placing of rock blocks into a specific space domain is the most significant step of random structure modeling for SRM

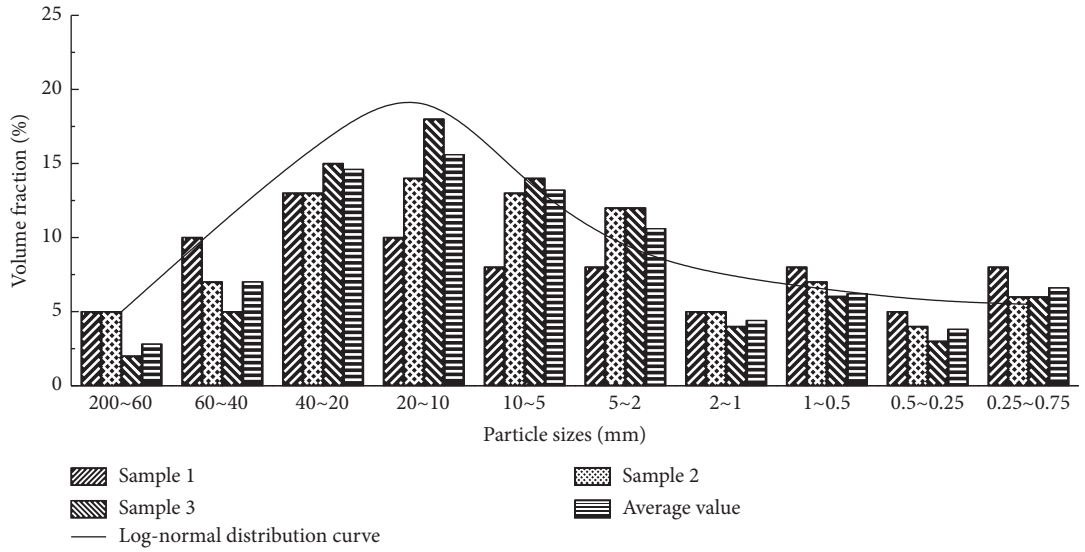

Figure 1: Typical granulometric curve of SRM.

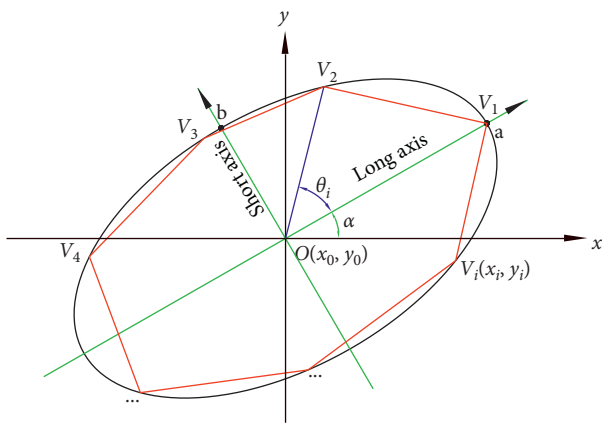

Figure 2: Random geometric shape of rock blocks.

samples with statistical characteristic. Such steps can be divided into four substeps: random translation, invasion judgment, position adjustment, and data storage, among which the substep of strict invasion judgment is the core of the placing process. Considering that the mutual invasion of rock blocks can be judged by the relative position of the vertexes and edges of random polygons, the invasion judgment of rock blocks on a plane can be solved by the geometric vector method.

(1) Judgment of Central Position. This process actually is a simplified judgment of vertex invasion. The aim of this process is to ensure that all vertexes of a new placing polygon are within the user-specified region. If the coordinate of a vertex is beyond the region boundary, the central position of the polygon executes geometric translation according to the horizontal or vertical distance between the vertex and the region boundary.

(2) Judgment of Vertex Invasion. Currently, there have been many methods for judgment of vertex invasion, such as sum of intersection angles, sum of triangle areas, and vector cross product [43]. In this study, the method of the vector cross product is used for invasion judgment of rock blocks. The core idea of this method is to create two new vectors and carry out a vector cross product. These two vectors set one judging vertex of the new placing polygon as the starting point and each two adjacent vertexes of the placed polygon as the ending point. Considering that the vertexes of each polygon are arranged in order along the counterclockwise direction, the judging vertex can be determined within the placed polygon once the value of the vector cross product is equal to or greater than zero. The situation of the judging vertex on the edges of the placed polygon is regarded as the judging vertex within the placed polygon here. Once the value of the vector cross product is equal to or greater than zero, the central position of the placing polygon needs to be replaced. Only when all values of vector cross products for the new placing polygon is less than zero, the new placing polygon does not invade the placed polygon.

(3) Judgment of Edge Invasion. In fact, even if all vertexes of the new placing polygon have no invasion to the placed polygon, the edge invasion may still exist, as shown in Figure 3. To solve this problem, the intersection judgment of two line segments is a quite effective way. If we use the vector $\overrightarrow{\mathbf{AB}}$ denoting one edge of the placing polygon and the vector $\overrightarrow{\mathbf{CD}}$ denoting one edge of the placed polygon, the situation of **A** and **B** located at the two sides of the edge **CD** yields

$$(\overrightarrow{\mathbf{CD}} \times \overrightarrow{\mathbf{CA}}) \cdot (\overrightarrow{\mathbf{CD}} \times \overrightarrow{\mathbf{CB}}) < 0. \tag{17}$$

Similarly, the situation of **C** and **D** located at the two sides of the edge **AB** yields

$$(\overrightarrow{\mathbf{AB}} \times \overrightarrow{\mathbf{AC}}) \cdot (\overrightarrow{\mathbf{AB}} \times \overrightarrow{\mathbf{AD}}) < 0. \tag{18}$$

Evidently, the edge invasion will occur when the above two situations are satisfied.

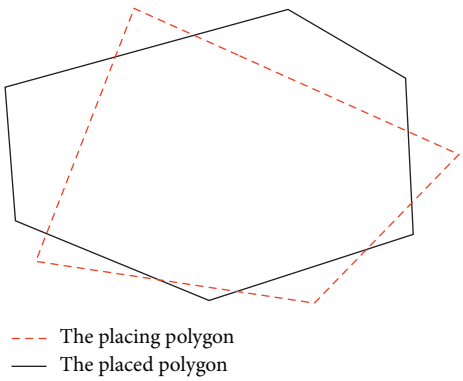

Figure 3: Situation of edge invasion.

Figure 4 presents the flow chart of random structure modeling of SRM, which can achieve random structure models of SRM with different rock block proportions and inclinations.

4. Deformation and Failure Simulation of SRM

4.1. Numerical Modeling and Parameter Selection. Particle flow code (PFC), proposed by Cundall and Strack (1979), is an advanced multithreaded discontinuum code and can simulate the initiation and growth of local microcracks by the interactions and movements of particles [44]. Therefore, it is quite suitable to simulate the deformation and failure of granular materials like SRM. In this study, the geometric model of SRM with random structures in size of $40\,\text{cm} \times 80\,\text{cm}$ will be generated following the above flow chart first, and then the model region beyond all rock blocks (this region is actually the part of fine soils) will be fully filled by small particles with diameters of 0.8–1.2 mm. The model region within all rock blocks will be replaced by the clump template pebbles via the bubble pack algorithm of Taghavi et al. [45]. The ratio of the smallest to the largest pebble in the clump is set as 0.3. The distance corresponding to an angular measure of smoothness in degrees is 150. The closest distance from the pebble center to the clump's geometric boundary is greater than one-fifth of the pebble radius.

Assembling the particle modules of fine soils and rock blocks together, the final particle model of SRM can be established, as shown in Figure 5. Considering that the most of SRM in practical engineering is always distributed near the earth surface or be used as a filling material, the confining pressure of them is relatively low, and they may lose stability under their own weight, a low confining pressure of 1 kPa will be applied on the surface of samples before the uniaxial compression test for obtaining the initial isotropic consolidated samples. Due to the low confining pressure and the cohesion of soil, the consolidated samples can still be kept stable when the confining pressure is removed. Therefore, when the consolidation process is completed, a series of stress-controlled uniaxial compression tests for SRM with random structures are conducted, in which the bottom boundary of the model is fixed, while uniformly distributed vertical loadings are applied on the top boundary. The necessary parameters of fine soils and rock blocks for numerical simulation are shown in Table 1.

4.2. Deformation and Failure Simulation. Figure 6 indicates that the bond failure between particles will occur at the densely placed area of rock blocks with the increase of uniformly distributed loading (rock block proportion is of 40%). When the uniformly distributed loading is gradually approaching the bearing capacity of SRM, the bond failure zone continuously extends, which actually implies that the deformation plays a major role in this stage. When the uniformly distributed loading reaches the bearing capacity of SRM, a clear band of bond failure throughout boundaries is formed. At that time, SRM really failed.

Figure 7 shows that the axial and lateral strain of SRM approximately takes on a linear relationship with the increase of uniformly distributed loading before the SRM reaches its bearing capacity. When the uniformly distributed loading reaches more than about 90% of bearing capacity, the axial and lateral strain of SRM increases sharply. When the uniformly distributed loading approaches the bearing capacity of SRM, the axial and lateral strains do not converge any more. At that time, this uniformly distributed loading thus can be regarded as the bearing capacity of SRM.

Figure 8 shows that when the uniformly distributed loading reaches the bearing capacity of SRM, the shear strain will not converge, which implies that SRM has been really destroyed. Therefore, the ultimate shear strain of SRM can be determined according to equation (4). Here, the value of the ultimate shear strain of SRM with rock block proportion of 40% is about 0.08×10^{-2}.

5. Discussion

5.1. Impact of Rock Block Proportion on Ultimate Shear Strain. Since the proportion of rock blocks has a significant impact on the physical and mechanical properties of SRM, it is bound to affect the bearing capacity of SRM. Figure 9 shows that the bond failure between soil particles appears a significant phenomenon of getting round rock blocks. The bond failure zones between soil particles are expending with the increase of rock block proportion. Particularly, when the rock block proportion is relatively high, the bond failure zones between soil particles will almost fill the whole SRM sample. The results shown in Figure 9 also present that the higher rock block proportion may lead to the more serious block. The reason may be that the shear band of SRM with high rock block proportion has a broader affected area. Figure 10 indicates that the ultimate shear strain changes exponentially with the increase of rock block proportion in spite of a certain discreteness in the case of high rock block proportion.

5.2. Impact of Rock Block Inclination on Ultimate Shear Strain. Due to long geological deposition, the inclination of rock blocks within natural SRM may have orientated distribution features, leading to an obvious stratification in structure and a more prominent anisotropy in mechanical

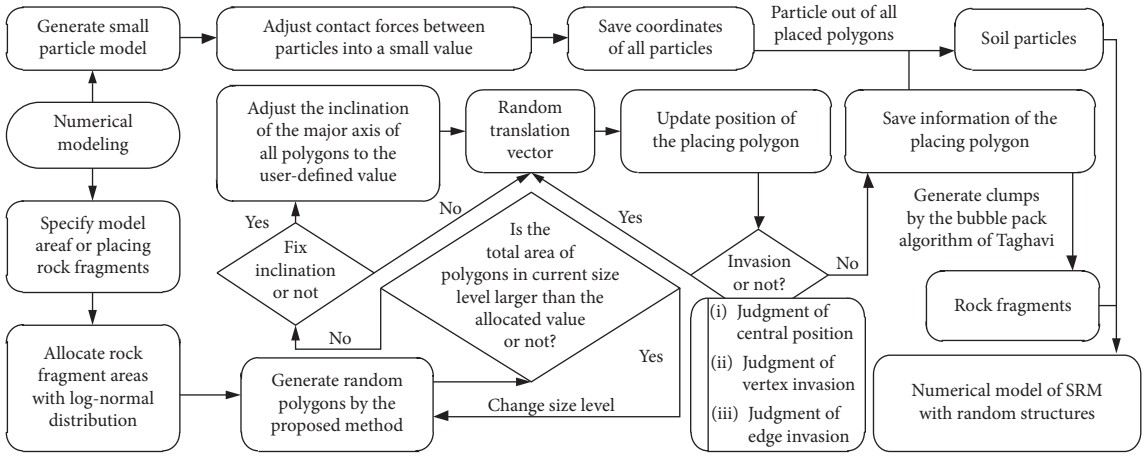

Figure 4: Flow chart of random structure modeling of SRM.

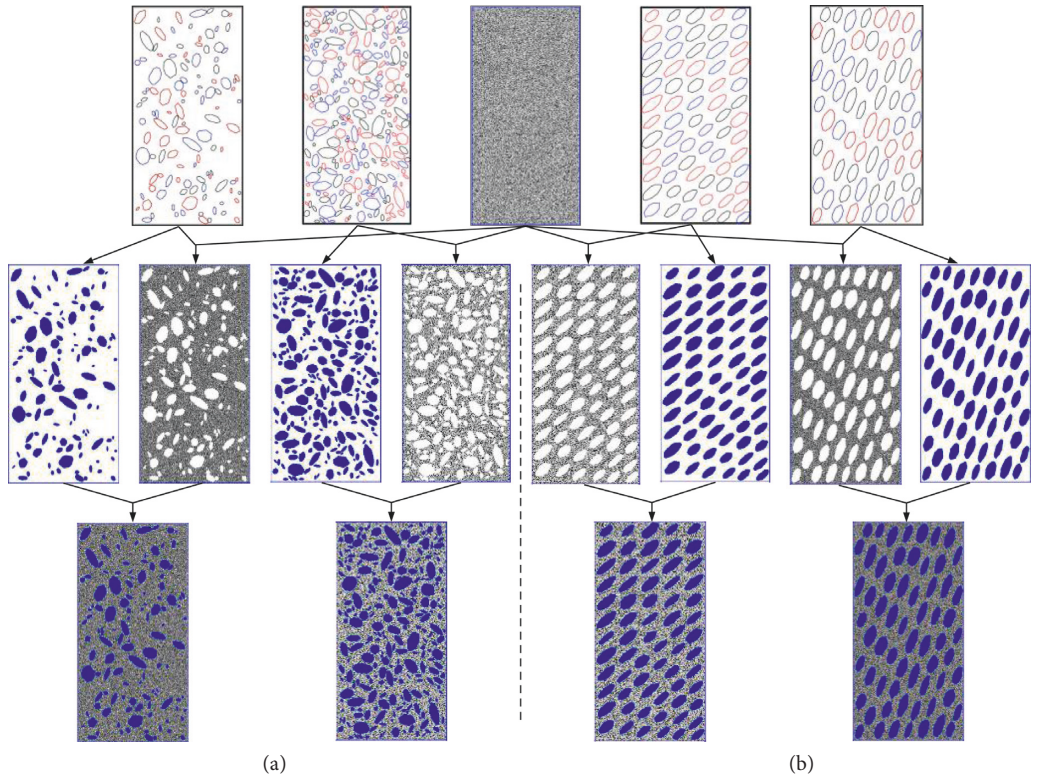

Figure 5: Random models of SRM with different rock block proportions (a) and inclinations (b).

Table 1: Numerical parameters of soil particles and rock blocks.

Parameter list	Soil particles	Rock blocks
Density (kg/m^3)	2050	2300
Effective deformability modules (Pa)	1.0*e*8	5.0*e*9
Normal-to-shear stiffness ratio	3.5	4.33
Frictional coefficient	0.5	0.5
Bond effective modulus (Pa)	1.0*e*8	
Bond normal-to-shear stiffness ratio	3.5	
Tensile strength (Pa)	1.0*e*5	
Cohesion (Pa)	5.0*e*5	
Friction angle (°)	30.0	

property. Therefore, the deformation and failure of SRM are more likely to occur along the direction of stratification. In order to study the impact of rock block inclination on the deformation and failure of SRM, random structure models with user-specified rock block inclination and 40% of rock block proportion are established. Results of numerical simulation as shown in Figure 11 present that when the rock block inclinations lie between 20° and 80°, the distribution of bond failure zones has an obvious bedding phenomenon, as well as a good consistency with rock block inclinations. The SRM with rock block inclination closer to 45° has a relatively

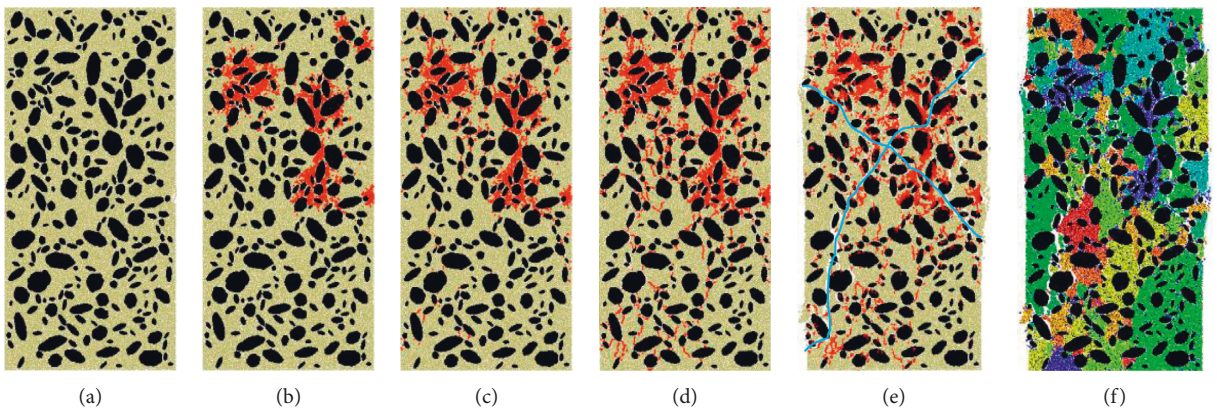

Figure 6: Expanding of bond failure between particles with increase of uniformly distributed loading. (a) 0 kPa. (b) 50 kPa. (c) 100 kPa. (d) 120 kPa. (e) 132 kPa. (f) Destroyed.

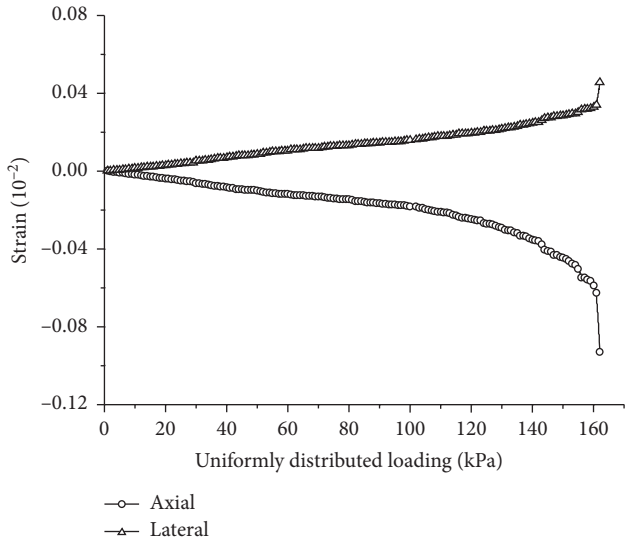

Figure 7: Changes of axial and lateral strains with increase of uniformly distributed loading.

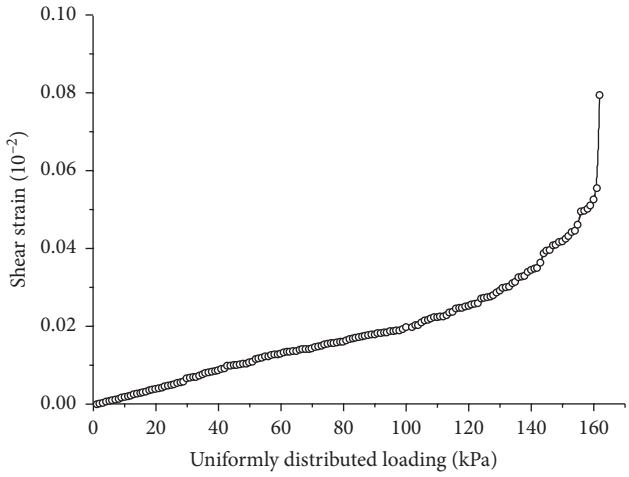

Figure 8: Changes of shear strain with increase of uniformly distributed loading.

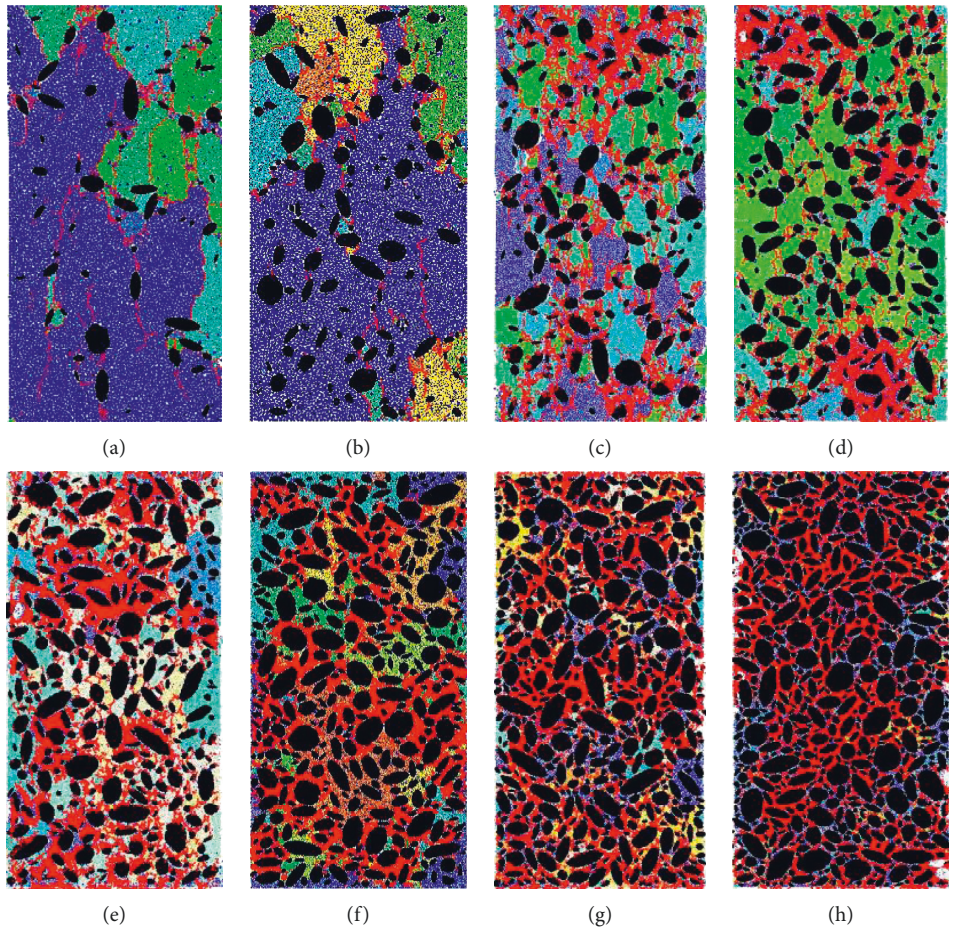

Figure 9: Distributions of bond failure zones under different rock block proportions. (a) 10%. (b) 20%. (c) 30%. (d) 40%. (e) 50%. (f) 60%. (g) 70%. (h) 80%.

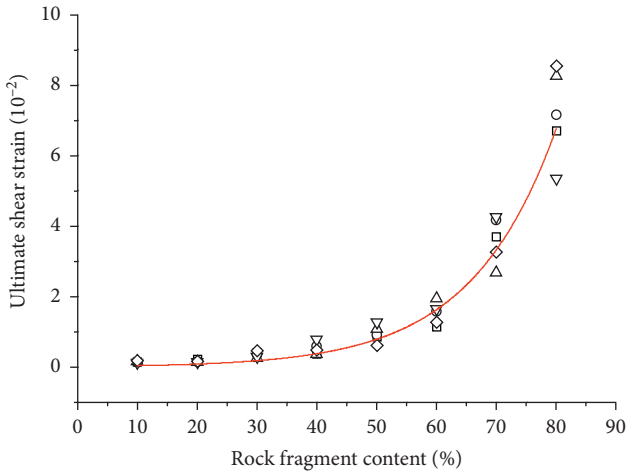

Figure 10: Relationship between ultimate shear strain and rock block proportion.

small affected area and a slight block. Figure 12 indicates that the ultimate shear strain changes with the increase of rock block inclination like a w-shape in spite of data discreteness caused by rock block size. The main reason why the ultimate shear strain of SRM with the rock block inclinations of 0° and 90° are relatively high may be that the slenderized rock blocks in horizontal or vertical directions increase the length of the shear failure path.

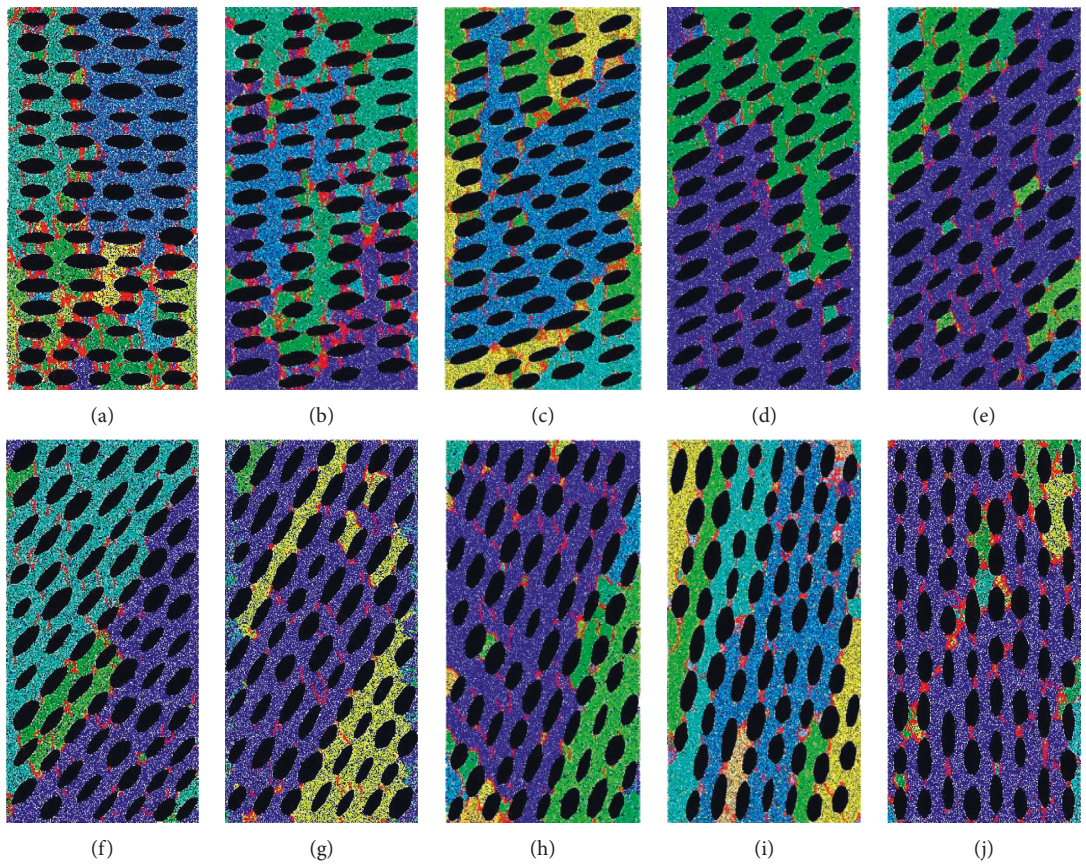

Figure 11: Distribution of the bond failure zone under different rock block inclinations. (a) 0°. (b) 10°. (c) 20°. (d) 30°. (e) 40°. (f) 50°. (g) 60°. (h) 70°. (i) 80°. (j) 90°.

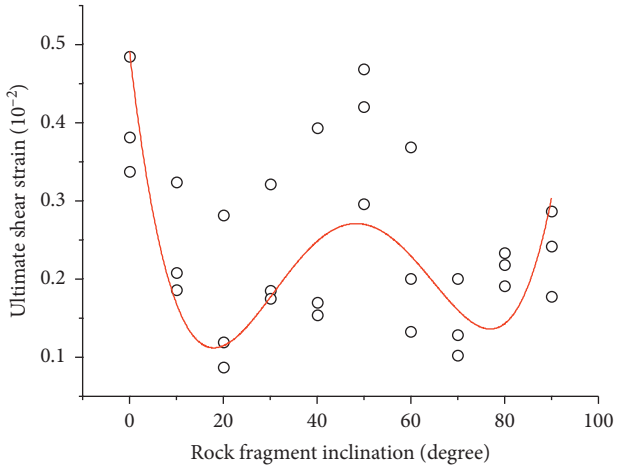

Figure 12: Relationship between ultimate shear strain and rock block inclination.

5.3. Impact of Cementation Degree on Ultimate Shear Strain. Due to different deposition time and geophysical environment, different cementing forms within SRM may also appear, such as argillaceous, calcareous, and siliceous. When the degree of cementation between particles is strong, the property of SRM may be like the concrete. When the degree of cementation between particles is weak, the property of SRM is like the loose coarse soil. Therefore, different degrees of cementation between particles may cause different deformations and failures. Random structure models of SRM with specified rock block proportion and inclination but different cementation degrees have been used in the stress-controlled uniaxial compression test (here different bond effective moduli are used to characterize the cementation

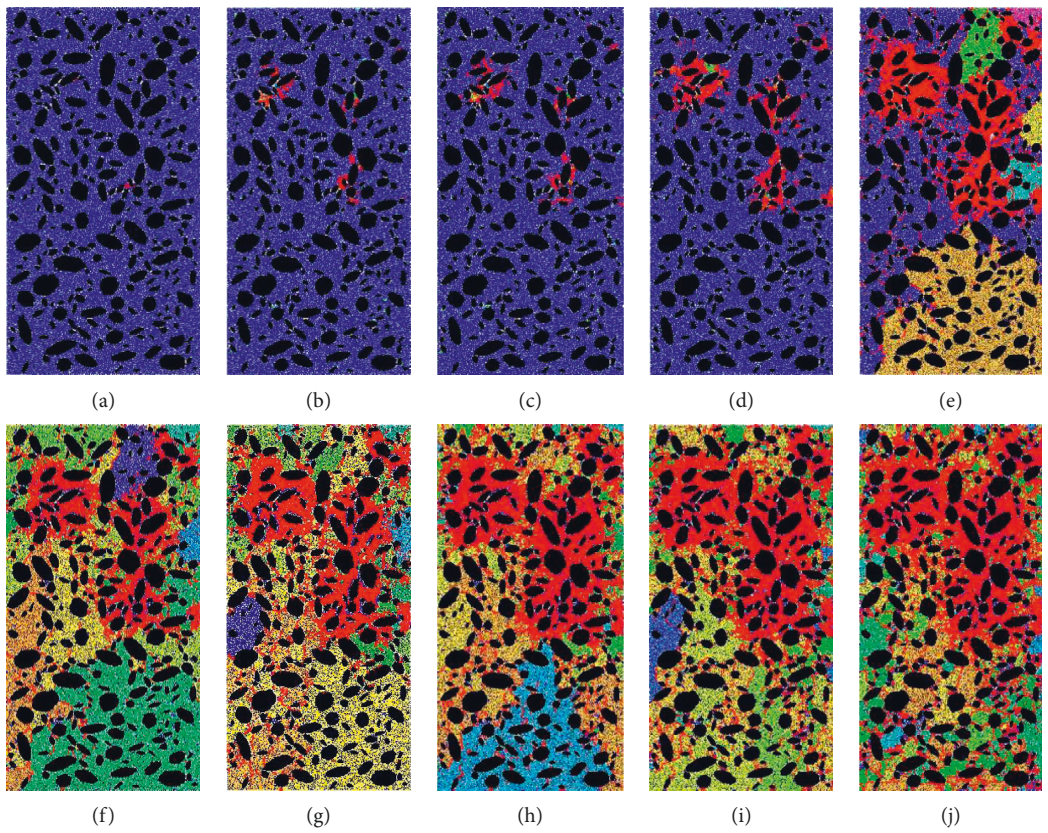

Figure 13: Distribution of the bond failure zone under different cementation degrees between particles. (a) 1*E*6. (b) 5*E*6. (c) 1*E*7. (d) 5*E*7. (e) 1*E*8. (f) 5*E*8. (g) 1*E*9. (h) 5*E*9. (i) 1*E*10. (j) 5*E*10.

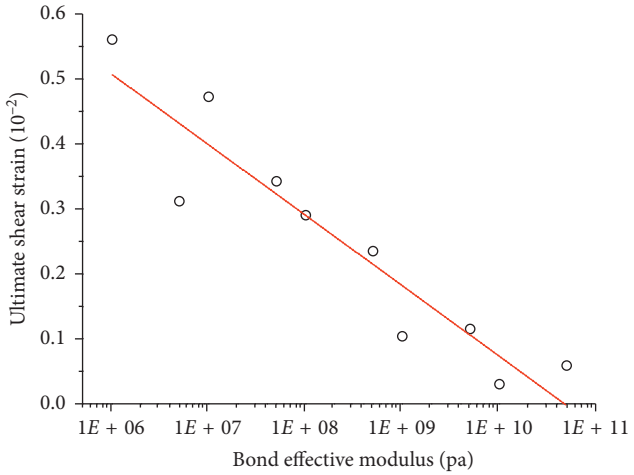

Figure 14: Relationship between ultimate shear strain and cementation degree between particles.

degree between soil particles). Simulation results, as shown in Figure 13, present that the bond failure zones expand with the increase of cementation degree between particles. The higher the cementation degree is, the more the bond failure zones are. The more serious the block will occur when the cementation degree between particles gets strong. Figure 14 indicates that the ultimate shear strain decreases with the increase of the cementation degree between particles. The data discreteness maybe mainly caused by the rock block proportion within the shear band.

6. Conclusions

Soil-rock mixture is a kind of complex geomaterial because of its random composition and structure. In this study, the deformation and failure characteristics of the soil-rock mixture with different compositions and structures had been discussed by a series of numerical uniaxial compression tests. Results indicate that there was a significant phenomenon of getting round rock blocks occurring in the deformation and failure process. The ultimate shear strain increased exponentially with the increase of rock block proportion but decreased with the increase of cementation degree between particles. The obvious bedding phenomena always appeared in the direction of rock block inclination. The size and shape of rock blocks caused the discreteness of ultimate shear strain and induced more tortuous shear failure path. Therefore, the ultimate shear strain changed like a w-shape with the increase of rock block inclination. This work can provide theoretical and technical references for engineering safety and comprehensive reinforcement of SRM.

Data Availability

The data used to support the findings of this study are available from the corresponding author upon request.

Disclosure

All authors whose names appear on the submission have contributed sufficiently to the scientific work and therefore share collective responsibility and accountability for the results.

Conflicts of Interest

The authors declare that there are no conflicts of interest regarding the publication of this paper.

Acknowledgments

The study was supported by the Natural Science Foundation of Jiangsu Province (BK20171006), National Key R&D Program of China (2017YFC150110), and China Postdoctoral Science Foundation Funded Project (2017M620838).

References

[1] X. Li, Q. L. Liao, and J. M. He, "In-situ tests and a stochastic structural model of rock and soil aggregate in the three gorges reservoir area, China," *International Journal of Rock Mechanics and Mining Sciences*, vol. 41, no. 3, pp. 702–707, 2004.

[2] R. Huang, "Mechanisms of large-scale landslides in China," *Bulletin of Engineering Geology and the Environment*, vol. 71, no. 1, pp. 161–170, 2012.

[3] S. N. Wang, C. Shi, W. Y. Xu, H. L. Wang, and Q. Z. Zhu, "Numerical direct shear tests for outwash deposits with random structure and composition," *Granular Matter*, vol. 16, no. 5, pp. 771–783, 2014.

[4] W. G. Holtz and H. J. Gibbs, "Triaxial shear tests on pervious gravelly soils," *Journal of the Soil Mechanics and Foundations Division*, vol. 82, no. 1, pp. 1–22, 1956.

[5] R. J. Chandler, "The inclination of talus, arctic talus terraces, and other slopes composed of granular materials," *The Journal of Geology*, vol. 81, no. 1, pp. 1–14, 1973.

[6] Q. Zhai, H. Rahardjo, and A. Satyanaga, "Variability in unsaturated hydraulic properties of residual soil in Singapore," *Engineering Geology*, vol. 209, pp. 21–29, 2016.

[7] E. W. Medley, "Estimating block size distributions of Melanges and similar block-in-matrix rocks (bimrocks)," in *Proceedings of 5th North American Rock Mechanics Symposium (NARMS)*, pp. 509–606, University of Toronto Press, Toronto, Canada, July 2002.

[8] S. W. Tyler and S. W. Wheatcraft, "Fractal scaling of soil particle-size distributions: analysis and limitations," *Soil Science Society of America Journal*, vol. 56, no. 2, pp. 362–369, 1992.

[9] N. Coli, P. Berry, and D. Boldini, "In situ non-conventional shear tests for the mechanical characterisation of a bimrock," *International Journal of Rock Mechanics and Mining Sciences*, vol. 48, no. 1, pp. 95–102, 2011.

[10] W. J. Xu, Q. Xu, and R. L. Hu, "Study on the shear strength of soil–rock mixture by large scale direct shear test," *International Journal of Rock Mechanics & Mining Sciences*, vol. 48, no. 8, pp. 1235–1247, 2011.

[11] H. F. Zhao and L. M. Zhang, "Effect of coarse content on shear behavior of unsaturated coarse granular soils," *Canadian Geotechnical Journal*, vol. 51, no. 12, pp. 1371–1383, 2014.

[12] W.-J. Chang and T. Phantachang, "Effects of gravel content on shear resistance of gravelly soils," *Engineering Geology*, vol. 207, pp. 78–90, 2016.

[13] S. Huang, X. Ding, Y. Zhang, and W. Cheng, "Triaxial test and mechanical analysis of rock-soil aggregate sampled from natural sliding Mass," *Advances in Materials Science and Engineering*, vol. 2015, Article ID 238095, 14 pages, 2015.

[14] B. Seif El Dine, J. C. Dupla, R. Frank, J. Canou, and Y. Kazan, "Mechanical characterization of matrix coarse-grained soils with a large-sized triaxial device," *Canadian Geotechnical Journal*, vol. 47, no. 4, pp. 425–438, 2010.

[15] Z. Zhou, H. L. Fu, B. C. Liu et al., "Experimental study of the permeability of soil-rock-mixture," *Journal of Hunan University*, vol. 33, no. 6, pp. 25–28, 2006.

[16] H. Rahardjo, I. G. B. Indrawan, E. C. Leong, and W. K. Yong, "Effects of coarse-grained material on hydraulic properties and shear strength of top soil," *Engineering Geology*, vol. 101, no. 3-4, pp. 165–173, 2008.

[17] I. G. B. Indrawan, H. Rahardjo, and E. C. Leong, "Effects of coarse-grained materials on properties of residual soil," *Engineering Geology*, vol. 82, no. 3, pp. 154–164, 2006.

[18] S. N. Wang, *Study on Deformation Failure and Movement Simulation for Large-Scale Glacial Deposits*, Hohai University, Nanjing, China, 2016.

[19] L. E. Vallejo, "Interpretation of the limits in shear strength in binary granular mixtures," *Canadian Geotechnical Journal*, vol. 38, no. 5, pp. 1097–1104, 2001.

[20] M. A. Hossain and J.-H. Yin, "Shear strength and dilative characteristics of an unsaturated compacted completely decomposed granite soil," *Canadian Geotechnical Journal*, vol. 47, no. 10, pp. 1112–1126, 2010.

[21] G. O. Bogado and F. M. Francisca, "Shear wave propagation in residual soil-rigid inclusion mixtures," *Powder Technology*, vol. 343, no. 2, pp. 595–598, 2019.

[22] M. Afifipour and P. Moarefvand, "Mechanical behavior of bimrocks having high rock block proportion," *International Journal of Rock Mechanics and Mining Sciences*, vol. 65, no. 1, pp. 40–48, 2014.

[23] Y. Zheng, "Development and application of numerical limit analysis for geological materials," *Chinese Journal of Rock Mechanics & Engineering*, vol. 31, no. 7, pp. 1297–1316, 2012.

[24] Y. Zheng and L. Kong, *Geotechnical Plastic Mechanics*, China Architecture and Building Press, Beijing, China, 2010.

[25] G. Hong, *Study on the Criterion of Yield and Failure for Geomaterials*, Institute of Rock and Soil Mechanics, Chinese Academy of Sciences, Wuhan, China, 2007.

[26] H. Matsuoka, Y. Yao, and D. Sun, "The cam-clay models revised by the SMP criterion," *Soils and Foundations*, vol. 39, no. 1, pp. 81–95, 1999.

[27] Q. Yang, X. Chen, and W. Y. Zhou, "An anisotropic yield criterion based on the two-order fabric tensor," *Engineering Mechanics*, vol. 22, no. 6, pp. 15–20, 2005.

[28] P. V. Lade, "Elastoplastic stress-strain theory for cohesionless soil," *International Journal of Solids and Structures*, vol. 13, no. 11, pp. 1037–1053, 1977.

[29] M. J. Roy, R. J. Klassen, and J. T. Wood, "Evolution of plastic strain during a flow forming process," *Journal of Materials Processing Technology*, vol. 209, no. 2, pp. 1018–1025, 2009.

[30] J. Faleskog and I. Barsoum, "Tension-torsion fracture experiments-part I: experiments and a procedure to evaluate the equivalent plastic strain," *International Journal of Solids & Structures*, vol. 50, no. 25-26, pp. 4241–4257, 2013.

[31] X. Mou, K. Peng, J. Zeng, L. L. Shaw, and K.-W. Qian, "The influence of the equivalent strain on the microstructure and

hardness of H62 brass subjected to multi-cycle constrained groove pressing," *Journal of Materials Processing Technology*, vol. 211, no. 4, pp. 590–596, 2011.

[32] J. Polak, "Plastic strain-controlled short crack growth and fatigue life," *International Journal of Fatigue*, vol. 27, no. 10–12, pp. 1192–1201, 2005.

[33] L. Jie, Z. Yingren, T. Xiaosong et al., "Application of rock and soil's dynamic limit strain criterion in stability analysis of slope engineering," *Journal of Vibration and Shock*, vol. 35, no. 17, pp. 13–18, 2016, in chinese.

[34] E. Abi, X. Feng, Y. Zheng et al., "Strain analysis and numerical analysis based on limit strain for geomaterials," *Chinese Journal of Rock Mechanics & Engineering*, vol. 34, no. 8, pp. 1552–1560, 2015.

[35] H. Gao, Y. Zheng, and X. Feng, "Deduction of failure criterion for geomaterials based on maximum principal shear strain," *Chinese Journal of Rock Mechanics & Engineering*, vol. 26, no. 3, pp. 518–524, 2007.

[36] E. S. Lindquist and R. E. Goodman, "Strength and deformation properties of a physical model melange," in *Proceedings 1st North American Rock Mechanics Symposium*, pp. 843–850, American Rock Mechanics Association, Austin, TX, USA, June 1994.

[37] E. S. Lindquist, *The Strength and Deformation Properties of Melange*, University of California, Berkeley, CA, USA, 1994.

[38] E. W. Medley, "Systematic characterization of mélange bimrocks and other chaotic soil/rock mixtures," *FELSBAU Rock and Soil Engineering*, vol. 17, no. 3, pp. 152–162, 1999.

[39] X. You, *Stochastic Structural Model of the Earth-Rock Aggregate and its Application*, Beifang Jiaotong University, Beijing, China, 2001, in Chinese.

[40] X. Wang and X. L. Ding, "Numerical tests on impact of stone content to mechanical parameters of soil-rock mixture," *Port & Waterway Engineering*, vol. 2010, no. 10, pp. 93–99, 2010, in chinese.

[41] J. He, X. Li, S. Li, J. Gu, and Y. Yin, "Numerical study of rock-soil aggregate by discrete element modeling," in *Proceedings of the International Conference on Fuzzy Systems & Knowledge Discovery*, pp. 565–569, IEEE, Tianjin, China, August 2009.

[42] W.-J. Xu, S. Wang, H.-Y. Zhang, and Z.-L. Zhang, "Discrete element modelling of a soil-rock mixture used in an embankment dam," *International Journal of Rock Mechanics and Mining Sciences*, vol. 86, pp. 141–156, 2016.

[43] D. Liu, Y. Wang, and G. Lv, "Topology determined between point and polygon based on vector algebra," in *Proceedings of the 2nd Conference on Environmental Science and Information Application Technology*, pp. 12–15, IEEE, Wuhan, China, July 2010.

[44] Itasca Consulting Group, *PFC2D (Particle Flow Code in 2 Dimensions)*, Itasca Consulting Group Inc., Minneapolis, MN, USA, 2004.

[45] R. Taghavi, S. R. Behling, and Y. Mochizuki, "Method for use in designing an arbitrarily shaped object," United States Patent 5453934, 1993.